Influence of film thickness on the properties of sprayed ZnO thin films for gas sensor applications

CrossMark

R. Mariappan [a,b,*], V. Ponnuswamy [a], P. Suresh [c], N. Ashok [b], P. Jayamurugan [b], A. Chandra Bose [d]

[a] Department of Physics, Sri Ramakrishna Mission Vidyalaya College of Arts and Science, Coimbatore 641 020, Tamil Nadu, India
[b] Department of Physics, Adhiyamaan College of Engineering, Hosur 635 109, Tamil Nadu, India
[c] Materials Research Centre, Indian Institute of Science, Bangalore 560 012, Karnadaka, India
[d] Department of Physics, National Institute of Technology, Tiruchirappalli 620 015, Tamil Nadu, India

ARTICLE INFO

ABSTRACT

Transparent conducting ZnO films were prepared at substrate temperature 400 °C with different film thicknesses by nebulizer spray pyrolysis method on glass substrates. XRD studies reveal that the films are polycrystalline in nature having hexagonal crystal structure with preferred grain orientations along (0 0 2) and (1 0 1) directions. The crystallite size increases along (0 0 2) plane with the thickness increase and attains a maximum 109 nm for 913 nm film thickness. Analysis of structural parameters indicates that the films having thickness 913 nm are found to have minimum dislocation density and strain values. The HRSEM measurements show that the surface morphology of the films also changes with film thickness. EDAX estimates the average atomic percentage ratio of Zn and O in the ZnO films. Optical studies reveal the band gap energy decrease from 3.27 to 3.14 eV with increase of film thickness. Room temperature PL spectra show the near-band-edge emission and deep-level emission due to the presence of defects in the ZnO thin films. Impedance spectroscopy analysis indicates that grain boundary resistance decreases with the increasing ammonia concentration up to 500 ppm and the maximum sensitivity is found to be 1.7 for 500 ppm of ammonia.

© 2014 Elsevier Ltd. All rights reserved.

* Corresponding author at: Department of Physics, Adhiyamaan College of Engineering, Hosur 635 109, Tamil Nadu, India. Tel.: +91 4344261016; fax: +91 4344260573.
E-mail address: marijpr@gmail.com (R. Mariappan).

1. Introduction

The application range of semiconductor gas sensors prepared out of metal oxides such as ZnO [1], TiO₂ [2], SnO₂ [3], In₂O₃ [4] because of good response at ambient conditions, inexpensiveness, high stability with long product life and simplicity in fabrication. At present, research interest has been shifted to thin film sensors [5]. Zinc oxide (ZnO) is a promising material for gas sensor applications because of its high sensitivity, high stability, suitability to doping, non-toxicity, abundance in nature and low cost [6]. However, thin films are more suitable for such sensors because the gas-sensing properties are related to the material surface where the gases are adsorbed and the surface reactions occur. This reaction modifies the concentration of charge carriers in the material, giving rise to a change in its electrical resistance, which is used for the purpose of gas detection [7]. Pure and doped ZnO thin films for detection of toxic pollutant gases, combustible gases and organic vapours, which is a subject of growing importance in both domestic and industrial environments, have been reported other researchers. A scheme of developing specific sensors for detecting to many gases like methanol [5], ethanol [8], acetone [9], LPG [10], CO [11], H₂S [12,13], optical [14], H₂ [15], NH₃ [15–19] gas sensors and observed that ZnO thin film sensors are sensitive to NH₃ selectively and insensitive to other said species at higher temperature (175 °C). Recently, Minh et al. suggested that a sensor based ZnO thin films exhibited high sensitivity to NH₃ [20]. To the best of our knowledge, very little work has been reported on the ZnO thin films to detect ammonia vapour. High sensitivity gas sensor of ZnO thin films has been prepared by variety of techniques, such as chemical bath deposition [21], sol–gel dip coating method [22], co-evaporation [23], radio-frequency (RF) magnetron sputtering [24], successive ionic layer adsorption and reaction [25], electrochemical deposition [26], ultrasonically spray pyrolysis [27], etc. Nebulizer spray technique is widely used because it is simple and economically viable techniques, which produce films of good quality for device applications. The preparation method for sensing material therefore plays an important role in the morphological characteristics and control over the particle size and surface area of the sensor.

In the present work the preparation and characterization of ZnO thin films by the nebulizer spray pyrolysis (NSP) technique has been reported. The films were characterized by X-ray diffraction (XRD), high resolution scanning electron microscopy (HRSEM), atomic force microscope (AFM), energy dispersive X-ray analysis (EDAX), UV–Vis–NIR spectroscopy, Photoluminescence spectroscopy and Impedance spectroscopy. The results are discussed and reported.

2. Experimental details

Analytical reagent grade (99.5% purity, Sigma Aldrich) zinc acetate dehydrate [Zn(CH₃COO)₂·2H₂O] was used to prepare zinc oxide (ZnO) thin films at 400 °C using the nebulizer spray pyrolysis technique with varied film thickness from 225 to 1138 nm. The nebulizer spray pyrolysis experimental set-up and the details on the procedure for the depositing Sn doped ZnO thin films have been described elsewhere [28]. The spray nozzle was at a distance 5 cm from the substrate during deposition and solution flow rate was held constant at 0.5 ml/min. Air was used as the carrier gas maintained at a pressure of 30 psi. When aerosol droplets come close to the substrates, a pyrolytic decomposition process occurs and high quality ZnO films were produced. The spray solution was prepared with 0.1 M of zinc acetate dihydrate dissolved in 25 ml of de-ionized water and stirred for 10 min using a magnetic stirrer. The prepared solution was sprayed onto the ultrasonically cleaned glass substrates.

The thickness of ZnO films was measured using 'stylus profilometer'. The structural properties of the films were studied by X-ray diffraction (Bruker D8 advance X-ray diffractometer) with Cu Kα radiation (λ = 0.154 nm) in the $\theta/2\theta$ and the angle 2θ ranged from 20° to 80°. The optical studies of the films were done with a Ultra Violet–Visible–Near Infra Red (UV–Vis–NIR) spectrophotometer (Model JASCO-V-570) in the range 300–2500 nm. The room temperature photoluminescence (PL) spectrum was recorded with spectrofluorometer (Fluorolog Model FL3-11). Surface morphology for the films were characterized via high resolution scanning electron microscopy (HRSEM, FEI Quanta FEG 200) applying 30.0 kV operating voltage. The surface morphology was observed by an atomic force

microscope (CSPM4000) in contact mode. The composition of the films was analyzed by energy dispersive analysis using X-rays (EDAX) equipped in HRSEM, for which a 30 kV accelerating voltage was applied. Impedance measurements were performed using a Frequency Response, Solartron, Model 1360 coupled with the Solartron Dielectric Interface, 1296.

3. Results and discussion

3.1. X-ray diffraction analysis

The XRD patterns of the ZnO thin films deposited at 400 °C with different film thickness 225, 452, 681, 913 and 1138 nm are shown in Fig. 1a–e. X-ray diffraction spectra reveal the polycrystalline nature of the ZnO films with hexagonal crystal structure. Fig. 1 shows gradual change of preferential orientation of from (002) to (101) and additional peaks were recorded along (100), (102), (110), (103), (112) and (004) planes at temperature is considered to be developed in order to reduce the increased strain energy resulting from the more energetic impinging ions or could be due to increase in the film thickness from 225 to 913 nm. Orientation selection during the coalescence stage is more pronounced and is driven by a decrease in the total grain boundary area as well as minimization of interface and surface energy. Large grains with low surface and interface energy grow at the expense of smaller or unfavorably oriented grains. Texture in thin films is controlled by both nucleation and growth. During deposition process, interfacial energy will be lower for certain orientation(s) compared to other(s) and initial texture is driven by nucleation. However, as the deposition continues the growth will occur in such a way that interfacial and grain boundary energies are reduced. Grains with low free surface and interface energy density grow faster than grains in the other orientation and can occupy a large volume fraction of the film. The strain energy can also influence the orientation evolution at film
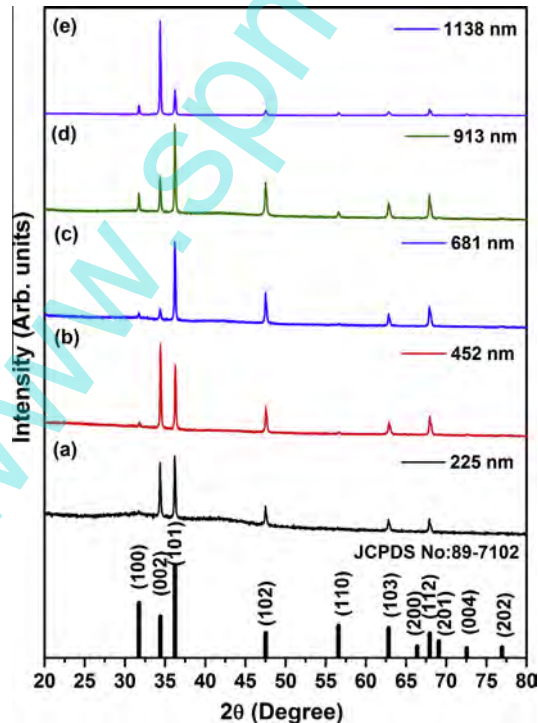
Fig. 1. X-ray diffraction patterns of ZnO thin films.

formation stage. However, in thin film which has high surface to volume ratios often this term is neglected taking surface as major contributor to the orientation change. Good agreement between the observed interplanar spacing "*d*" values of XRD reflections and the standard values of Joint Committee on the Powder Diffraction Spectra data (JCPDS No: 89-7102) has been confirmed in the ZnO phase. The lattice constant (*a*, *c*) was calculated using equation [28].

The variation of lattice constant (*a* and *c*) with different film thickness for ZnO films are listed in Table 1. It is observed that (Table 1) the lattice constant (*a* and *c*) value of ZnO thin film is slightly increased with the increased film thickness and well matches with Joint Committee on the Powder Diffraction Spectra data (JCPDS Card No. 89-7102). The dislocation density and micro strain were calculated using equations for the ZnO films [28].

The crystallite size of ZnO thin films were evaluated using equation [28]. The variation of crystallite size with film thickness of ZnO films are listed in Table 1. From Table 1, it is observed that the crystallite size increases along (0 0 2) plane with film thickness increase (1138 nm) and attains a maximum 109 nm at 400 °C. It is observed that Table 1, a sharp increase in crystallite size and decrease in dislocation density and microstrain with the film thickness. For film with thickness 1138 nm, the minimum values for dislocation density and microstrain probability of the film (Table 1) are obtained. It is concluded from the structural analysis that the increase of film thickness has a strong effect on the structural properties of the films.

Table 1
Structural parameters of ZnO thin films.

Film thickness (nm)	2θ	d-spacing (Å)	FWHM	(h k l) Crystal system	Lattice constants (Å)		Crystallite size nm	Dislocation density (δ) 10^{14} lin/m^2	Micro strain (ε) 10^4 lin^{-2} m^{-4}
					a	c			
225	31.586	2.832	0.897	100	3.2539	5.2080	11	108	35.3
	34.378	2.579	0.112	002			89	1.66	4.04
	36.209	2.480	0.074	101			133	0.73	2.54
	47.508	1.912	0.091	102			113	1.01	2.30
	62.815	1.479	0.149	103			74	2.36	2.72
	67.901	1.379	0.136	112			84	1.87	2.26
452	31.783	2.815	0.112	100	3.2489	5.2056	88	1.69	4.39
	34.418	2.603	0.114	002			87	1.72	4.10
	36.264	2.475	0.136	101			73	2.45	4.65
	47.560	1.910	0.091	102			113	1.01	2.30
	62.879	1.476	0.159	103			70	2.69	2.90
	67.952	1.378	0.136	112			84	1.87	2.26
681	31.735	2.819	0.149	100	3.2503	5.2098	66	5.68	5.86
	34.376	2.608	0.110	002			76	6.67	4.71
	36.214	2.480	0.112	101			89	1.70	3.82
	47.509	1.912	0.114	102			91	0.17	2.88
	62.844	1.477	0.136	103			81	0.59	2.49
	67.909	1.379	0.114	112			100	0.14	1.88
913	31.741	2.819	0.130	100	3.2516	5.2096	75	2.30	5.12
	34.375	2.608	0.093	002			106	1.15	3.36
	36.212	2.480	0.112	101			89	1.65	3.82
	47.511	1.912	0.091	102			113	1.01	2.30
	62.820	1.478	0.114	103			98	1.37	2.07
	67.919	1.378	0.114	112			100	1.29	1.88
1138	31.748	2.818	0.112	100	3.2517	5.2098	88	1.69	4.39
	34.382	2.606	0.091	002			109	1.10	3.28
	36.227	2.477	0.136	101			73	2.45	4.65
	47.520	1.911	0.136	102			75	2.27	3.46
	62.838	1.477	0.114	103			98	0.13	2.07
	67.922	1.378	0.136	112			84	1.87	2.26

3.2. SEM and AFM analysis

Fig. 2 shows the low magnification, high magnification and HRSEM images of the as grown ZnO thin films having different thickness. When the film thickness is 225 nm, a tiny chilly like structures is observed on glass substrate, however, the surface is well covered (Fig. 2a). Upon increasing the film thickness to 452 nm, these tiny chilly like structures become bigger and they are protuberant, as shown in Fig. 2b. Fig. 2c shows the HRSEM of the product with film thickness 681 nm and it is find that when more and more ZnO nanoflakes have formed and self assembled into clusters and substrate is well covered with these clusters and ZnO nanoflakes are very small. Further increase in the film thickness (913 nm) leads to an increased surface density of the clusters and nanoflakes, and they begin to grow upwards and finally connect each other (Fig. 2d). When the film thickness is 1138 nm (Fig. 2e), it is clearly observed that the nanoflake are tightly packed which may be attributed to the increase of film thickness. AFM images of ZnO films deposited onto glass substrates at 400 °C with different film thickness 225, 681 and 1138 nm are shown in Fig. 3a–c. The average roughness of films increases as
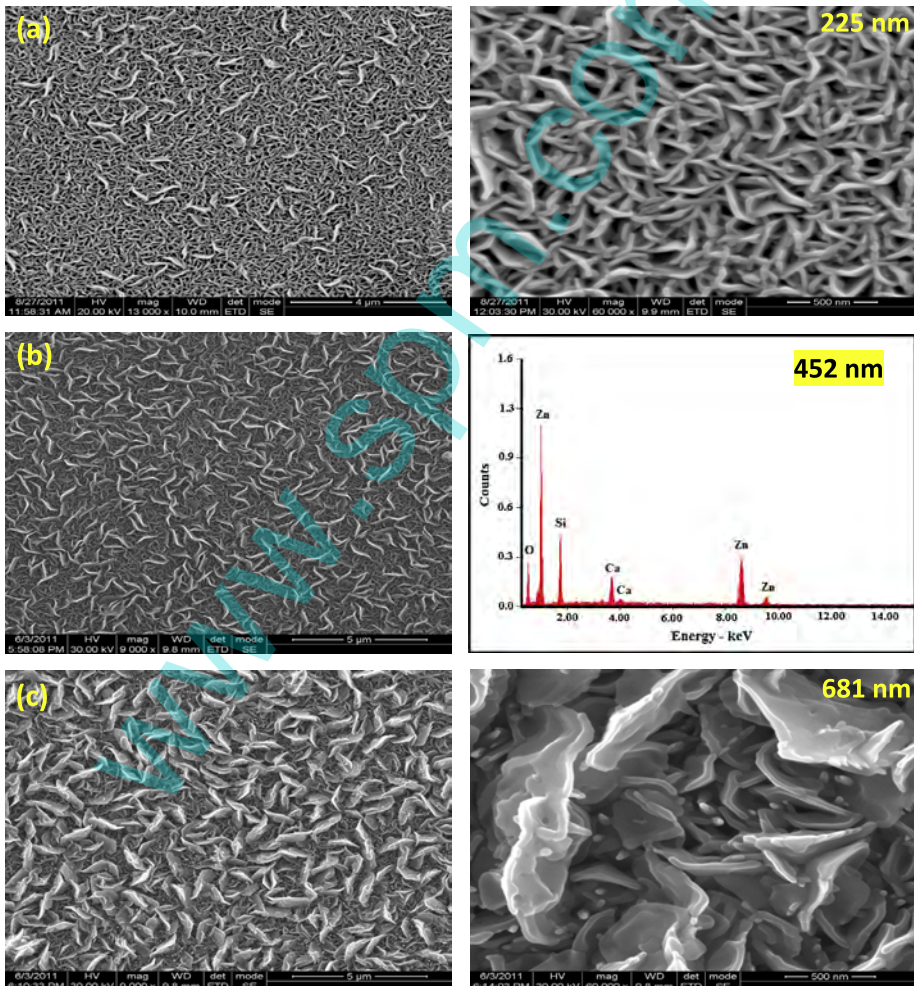
Fig. 2. High resolution SEM images of ZnO thin films (b) EDAX spectrum of ZnO thin films.
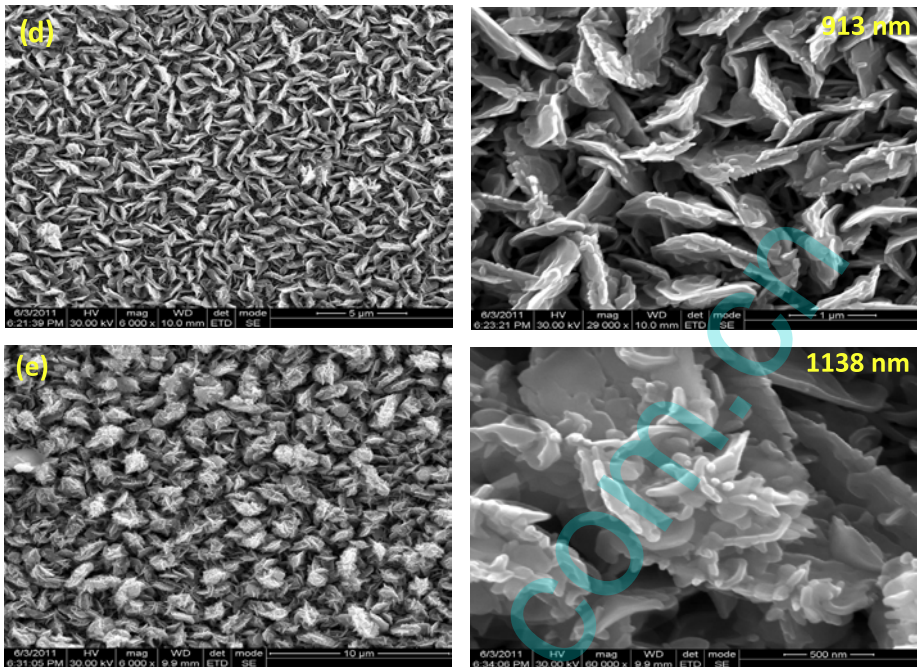
Fig. 2 (*continued*)

film thickness increases. The average roughness of ZnO films with different film thickness 225, 681 and 1138 nm are 8.26, 12.52 and 20.42 nm, respectively.

3.3. Compositional analysis

EDAX spectra of ZnO thin films deposited at 400 °C with film thickness (452 nm) are shown in Fig. 2b. The presence of the O peak at about 0.3 keV, the Zn peaks at 1.2, 8.5 and 9.5 keV, Si peak at 1.8 keV, Ca peak at 3.8 keV are observed in the spectra. These elements Si and Ca may probably include from the glass which is used as substrate. The film thickness increases with the increase of Zn atomic percentage while decreases with Si atomic percentage. It is seen from Table 2 (through EDAX analysis), the average atomic percentage of Zn and O is found to be 44.46 and 54.89 showing that the nebulizer sprayed ZnO thin films are nearly stoichiometric. They belong to the substrate or from the complex containing aqueous solution. The elemental composition of the ZnO films is presented in Table 2.

3.4. Optical properties

The transmittance spectra as a function of wavelength in the range 300–2500 nm for the four samples are shown in Fig. 4. The average transmittance in the visible region for the four samples is 92, 91, 84 and 72 respectively. When the film thickness increases from 225 to 1138 nm the transmittance is decreased. This may be due to the increased optical scattering caused by the increase of grain boundary and density owing to the large roughness in thicker films and oxygen vacancies resulted in decrease in optical transmittance. In order to better investigate the influence of the growth parameters on the absorption of the ZnO films, the recorded transmission spectra were employed for the determination of the optical energy gap (Eg).The band gap energy is calculated by using the following equation:
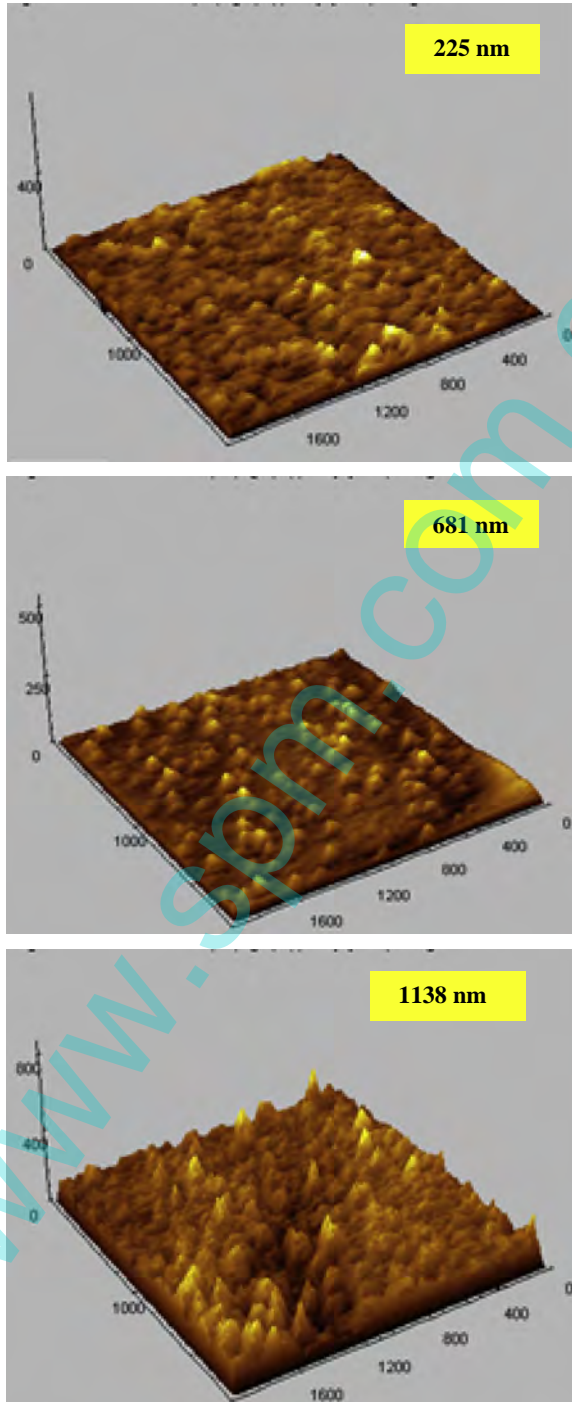
Fig. 3. AFM images of ZnO thin films.

Table 2
Variation of film thickness with atomic percentage for ZnO thin films.

Elements	Film thickness (nm)									
	225 nm		452 nm		681 nm		913 nm		1138 nm	
	Weight (%)	Atomic (%)	Weight (%)	Atomic (%)	Weight (%)	Atomic (%)	Weight (%)	Atomic (%)	Weight (%)	Atomic (%)
OK	29.21	52.98	27.58	53.23	22.42	50.89	20.78	50.14	16.48	44.46
ZnK	44.34	19.69	52.41	24.76	69.44	38.58	75.32	44.49	83.10	54.89
SiK	26.45	27.33	20.01	22.00	08.14	10.53	03.90	05.37	00.42	00.65
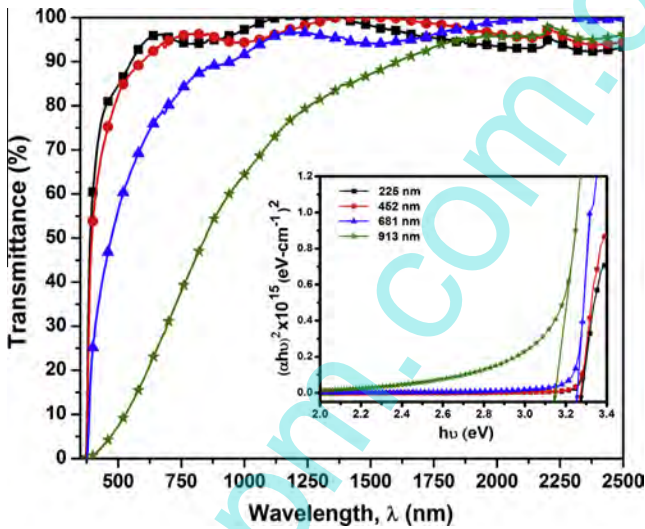
Fig. 4. Transmittance spectra of ZnO thin films (inset of this figure ($\alpha h\nu$) versus ($h\nu$) plots for ZnO thin films).

$$(\alpha h\nu)^n = A(h\nu - Eg)$$

where A is a constant, Eg the band gap energy and $n = 2$ for ZnO films which are direct band-gap semi-conductors. Assuming a direct transition between the edges of the valence and the conduction band, the variation of the absorption coefficient α with the photon energy $h\nu$ can be given by equation [29]. The optical band gap energy Eg of the films can be estimated by extrapolating the linear part of $(\alpha h\nu)^2$ versus $h\nu$ of the Tauc's plot shown in inset Fig. 4 and the same is found to be decreased from 3.27 to 3.14 eV due to the increase of film thickness. This means that the thickness also affects the bad gap of the film. A similar behavior was observed in ZnO films deposited by r.f. sputtering [30]. These results indicate that a tendency to a certain narrowing in the gap against the thickness occurs and the absorption edge is red shift in thicker films. In any case, there are several mechanisms that can cause the observed energy gap shifts, such as: (i) improvement or degradation of crystallinity, (ii) modifications in the height of the barrier due to change of the crystallite dimension, (iii) quantum size effects (iv) the density of impurities and (v) compressive or tensile strains.

3.5. Sample preparation of ZnO sensor device

Fig. 5a shows the schematic diagram of the prepared sensor device. The sensor is formed with a ZnO layer deposited on top of Indium tin oxide (ITO) substrate through NSP technique. The contacts, between which the resistance are made by sputtering of Au through a shadow mask. The distance
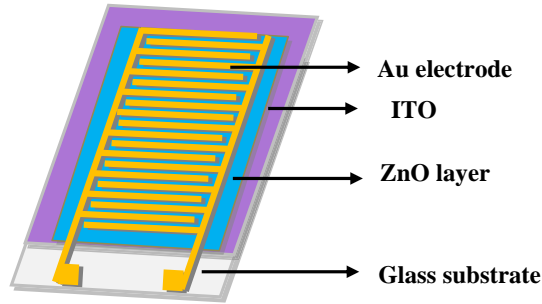
Fig. 5. Schematic diagram of ZnO sensor device.
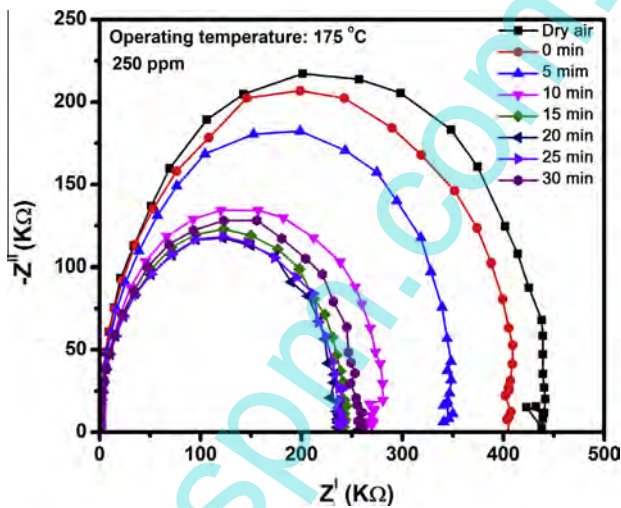
Fig. 6. Complex impedance studies of ZnO sensor device as a function of time.

between the Au electrodes was about 2 mm and thickness ~225 nm. Prior to deposition, the surface was cleaned in acetone for 15 min followed by ultrasonic treatment for another 15 min to remove organic contaminants. The impedance spectroscopy was carried out at different temperatures with an Ac voltage of 100 mV.

3.6. Ammonia gas sensing properties of ZnO device

Fig. 6 shows the real (Z') and imaginary (Z'') (Nyquist plots) parts of the in the complex impedance spectra and the corresponding equivalent circuits of ZnO gas sensor device deposited at 400 °C with film thickness (225 nm). At high frequency, the data show a semicircle indicating that the relaxation time of the bulk and the grain boundaries are close to each other. In the mid frequency range, a linear progress in the diffusion characteristics of ZnO is observed during insertion-desertion process. In the lowest frequency area, capacitive behavior is observed showing the characteristic response of a finite blocked diffusion. Centre of the semicircle is localized below real axis is ascribed to constant phase element. Intersect on the real axis of the semicircle at low frequencies is ascribed to the total resistance. Conversely, the impedance response of grain dominates at high frequencies and resistances of grain (R_g) is deduced from the left intersect of the semicircle to real axis. The intercept of semicircle

to real axis (Z') at low frequency depicts the sum of resistance of grains and grain boundaries while an intercept at high frequency depicts the resistance of grain only. Fig. 6 shows the effect of ammonia gas on the impedance of the sensor fixed at operating temperature 175 °C, concentration 250 ppm with different times. It is observed that the time increase has reduced the diameter of the circle. When the ZnO sensor surface is placed at the operating temperature 175 °C, the oxygen molecules from the ambient atmosphere accepts electrons to become O_2^-, O^-, or O^{2-} ions, thus decreasing the concentration of the number of charge carriers near the surface giving rise to a depletion region. This oxidation phenomenon helps in the removal of oxygen ion from ZnO surface leads to the decrease barrier height, thus increasing the conductance.

The sensitivity (S) of ZnO sensor was calculated as a function of frequency and ammonia concentration according to the following relationship:

$$S = \frac{Z_a}{Z_g}$$
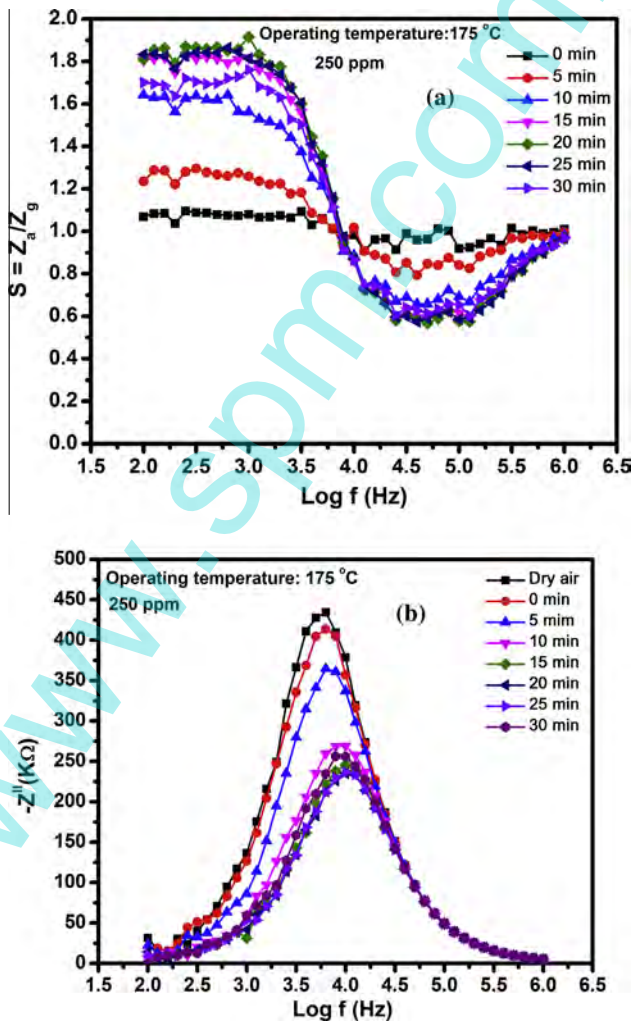
Fig. 7. (a) Variation of sensitivity with frequency of ZnO sensor device and (b) imaginary part of impedance with frequency of ZnO sensor device.

where Z_a and Z_g are the real part of the impedance for dry air atmosphere and or the ammonia atmosphere. Frequency dependence with sensitivity of ZnO sensor is shown in Fig. 7a. It can be observed that the sensitivity of the sensor remains constant within the frequency range 100 Hz–1 MHz, which is the range where the space charge transfer rules the conductivity process. The sensitivity decreases sharply as the frequency increases and becomes almost constant at a frequency higher than 1 MHz, in which the conductivity is controlled by the surface charge transfer of the grains. The maximum sensitivities are found to be 1.82 for 250 ppm of ammonia with time 20 min. These results indicate that the sensor can be tuned to achieve maximum sensitivity by selecting a suitable operating frequency range.

The plots of Z'' versus $\log f$ for ZnO sensor is shown in inset Fig. 7b. It can be seen that the values of Z'_{max} decrease with the increase of time indicating the loss decrease in the system. Besides, the peak frequency shifts towards higher frequencies and the peak height decreases with the increase of time. The peak broadening suggests the dependence of the relaxation process on the gas concentration 250 ppm.

3.7. Conclusion

Transparent conducting ZnO thin films were prepared by nebulizer spray pyrolysis technique on glass substrates using aqueous solution of 0.1 M zinc acetate dihydrate at 400 °C with different thickness. XRD analysis confirms that the ZnO films are polycrystalline in nature with hexagonal crystal structure having a preferred grain growth orientation along (0 0 2) and (1 0 1) planes. The presence of elemental constituents is confirmed from EDAX analysis. The average atomic percentage ratio of ZnO is found to be (44.46) Zn and (54.89) O with nearly stoichiometry. The increase in film thickness leads to the decrease in band gap energy from 3.27 to 3.14 eV. Hence the observed decrease in optical band gap energy can be directly attributed to the film thickness. The sensitivity of the sensor was found to be increased with time and maximum sensitivity is 1.82 at 400 °C (250 ppm). The investigation results of the prepared ZnO films ensure their stability and suitability for the development gas sensor devices.

References

[1] P.S. Shewale, G.L. Agawane, S.W. Shin, A.V. Moholkar, J.Y. Lee, J.H. Kim, M.D. Uplane, Thickness dependent H$_2$S sensing properties of nanocrystalline ZnO thin films derived by advanced spray pyrolysis, Sens. Actuators, B 177 (2013) 695–702.
[2] D. Meng, T. Yamazaki, T. Kikuta, Preparation and gas sensing properties of undoped and Pd-doped TiO$_2$ nanowires, Sens. Actuators, B 190 (2014) 838–843.
[3] C. Luan, K. Wang, Q. Yu, G. Lian, L. Zhang, Q. Wang, D. Cui, Improving the gas-sensing performance of SnO$_2$ porous nanosolid sensors by surface modification, Sens. Actuators, B 176 (2013) 475–481.
[4] P. Sowti Khiabani, E. Marzbanrad, C. Zamani, R. Riahifar, B. Raissi, Fabrication of In$_2$O$_3$ based NO$_2$ gas sensor through AC-electrophoretic depotion, Sens. Actuators, B 166–167 (2012) 128–134.
[5] V. Demarne, A. Grisel, An integrated low-power thin-film CO gas sensor on silicon, Sens. Actuators, B 13 (1988) 301.
[6] P.P. Sahay, R.K. Nath, Al-doped ZnO thin films as methanol sensors, Sens. Actuators, B 134 (2008) 654–659.
[7] J. Lagowski, E.S. Sproles Jr., H.C. Gatos, Quantitative study of the charge transfer in-chemisorption; oxygen chemisorption on ZnO, J. Appl. Phys. 60 (1977) 3566–3575.
[8] N.D. Khoang, D.D. Trung, N.V. Duy, N.D. Hoa, N.V. Hieu, Design of SnO$_2$/ZnO hierarchical nanostructures for enhanced ethanol gas-sensing performance, Sens. Actuators, B 174 (2012) 594–601.
[9] P.P. Sahay, Zinc oxide thin film gas sensor for detection of acetone, J. Mater. Sci. 40 (2005) 4383–4385.
[10] P. Mitra, H.S. Maiti, A wet-chemical process to form palladium oxide sensitizer layer on thin film zinc oxide based LPG sensor, Sens. Actuators, B 97 (2004) 49–58.
[11] J.F. Chang, H.H. Kuo, I.C. Leu, M.H. Hon, The effects of thickness and operation temperature on ZnO:Al thin film Co gas sensor, Sens. Actuators, B 84 (2002) 258–264.
[12] P.S. Shewale, V.B. Patil, S.W. Shin, J.H. Kim, M.D. Uplane, H$_2$S gas sensing properties of nanocrystalline Cu-doped ZnO thin films prepared by advanced spray pyrolysis, Sens. Actuators, B 186 (2013) 226–234.
[13] S.D. Shinde, G.E. Patil, D.D. Kajale, V.B. Gaikwad, G.H. Jain, Synthesis of ZnO nanorods by spray pyrolysis for H$_2$S gas sensor, J. Alloys Compd. 528 (2012) 109–114.
[14] A.O. Dikovska, P.A. Atanasov, S. Tonchev, J. Ferreira, L. Escoubas, Periodically structured ZnO thin films for optical gas sensor application, Sens. Actuators, A 140 (2007) 19–23.
[15] N.H. Al-Hardan, M.J. Abdullah, A. Abdul Aziz, Sensing mechanism of hydrogen gas sensor based on RF-sputtered ZnO thin films, Int. J. Hydrogen Energy 35 (2010) 4428–4434.
[16] H. Tang, M. Yan, H. Zhang, S. Li, X. Ma, M. Wang, D. Yang, A selective NH$_3$ gas sensor based on Fe$_2$O$_3$-ZnO nanocomposites at room temperature, Sens. Actuators, B 114 (2006) 910–915.

[17] G. Sberveglieri, S. Groppelli, P. Nelli, A. Tintinelli, G. Giunta, A novel method for the preparation of NH$_3$ sensors based on ZnO–In thin films, Sens. Actuators, B 24–25 (1995) 588–590.

[18] G. Sarala Devi, V. Bala Subrahmanyam, S.C. Gadkari, S.K. Gupta, NH$_3$ gas sensing properties of nanocrystalline ZnO based thick films, Anal. Chim. Acta 568 (2006) 41–46.

[19] V.A. Minh, L.A. Tuan, T.Q. Huy, V.N. Hung, N.V. Quy, Enhanced NH$_3$ gas sensing properties of a QCM sensor by increasing the length of vertically orientated ZnO nanorods, Appl. Surf. Sci. 265 (2013) 458–464.

[20] G.S. Trivikrama Rao, D. Tarakarama Rao, Gas sensitivity of ZnO based thick film sensor to NH$_3$ at room temperature, Sens. Actuators, B 55 (1999) 166–169.

[21] V.R. Shinde, T.P. Gujar, C.D. Lokhande, R.S. Mane, S.-H. Han, Use of chemically synthesized ZnO thin film as a liquefied petroleum gas sensor, Mater. Sci. Eng. B 137 (2007) 119–125.

[22] J. Kanungo, H. Saha, S. Basu, Pd sensitized porous silicon hydrogen sensor – influence of ZnO thin film, Sens. Actuators, B 147 (2010) 128–136.

[23] M.F. Al-Kuhaili, S.M.A. Durrani, I.A. Bakhtiari, Carbon monoxide gas-sensing properties of CeO$_2$–ZnO thin films, Appl. Surf. Sci. 255 (2008) 3033–3039.

[24] X. Zhou, Q. Xue, H. Chen, C. Liu, Current–voltage characteristics and ethanol gas sensing properties of ZnO thin film/Si heterojunction at room temperature, Physica E 42 (2010) 2021–2025.

[25] S.T. Shishiyanu, T.S. Shishiyanu, O.I. Lupan, Sensing characteristics of tin doped ZnO thin films as NO$_2$ gas sensor, Sens. Actuators, B 107 (2005) 379–386.

[26] P.K. Basu, P. Bhattacharyya, N. Saha, H. Saha, S. Basu, The superior performance of the electrochemically grown ZnO thin films as methane sensor, Sens. Actuators, B 133 (2008) 357–363.

[27] L.A. Patil, A.R. Bari, M.D. Shinde, V. Deo, Ultrasonically prepared nanocrystalline ZnO thin films for highly sensitive LPG sensing, Sens. Actuators, B 149 (2010) 79–86.

[28] R. Mariappan, V. Ponnuswamy, P. Suresh, Effect of doping concentration on the structural and optical properties of pure and tin doped zinc oxide thin films by nebulizer spray pyrolysis (NSP) technique, Superlattices Microstruct. 52 (2012) 500–513.

[29] U. Alver, T. Kilinc, E. Bacaksiz, T. kucukomeroglu, S. Nezir, I.H. Muthu, F. Aslan, Synthesis and characterization of spray pyrolysis zinc oxide microrods, Thin Solid Films 515 (2007) 3448–3451.

[30] M. Bouderbala, S. Hamzaoui, B. Amrani, Ali H. Reshak, M. Adnane, T. Sahraoui, M. Zerdali, Thickness dependence of structural, electrical and optical behavior of undoped ZnO thin films, Physica B 403 (2008) 3326–3330.